



HAL
open science

The April 2017 Mw6.5 Botswana Earthquake: An Intraplate Event Triggered by Deep Fluids

Blandine Gardonio, Romain Jolivet, Eric Calais, Henri Leclère

► **To cite this version:**

Blandine Gardonio, Romain Jolivet, Eric Calais, Henri Leclère. The April 2017 Mw6.5 Botswana Earthquake: An Intraplate Event Triggered by Deep Fluids. *Geophysical Research Letters*, 2018, 45 (17), pp.8886-8896. 10.1029/2018GL078297 . hal-02185463

HAL Id: hal-02185463

<https://hal.science/hal-02185463v1>

Submitted on 26 Aug 2019

HAL is a multi-disciplinary open access archive for the deposit and dissemination of scientific research documents, whether they are published or not. The documents may come from teaching and research institutions in France or abroad, or from public or private research centers.

L'archive ouverte pluridisciplinaire **HAL**, est destinée au dépôt et à la diffusion de documents scientifiques de niveau recherche, publiés ou non, émanant des établissements d'enseignement et de recherche français ou étrangers, des laboratoires publics ou privés.

13 **Abstract**

14 Large earthquakes in Stable Continental Regions (SCR) remain puzzling as, unlike at plate
15 boundaries, they do not result from the local build-up of strain driven by plate tectonics.
16 The 2017, M_w 6.5, Botswana normal-faulting earthquake occurred in a region devoid from
17 recent tectonic activity and where present-day deformation is negligible. The depth of the
18 event (29 ± 4 km), in a felsic lower crust where ductile deformation is expected, likely re-
19 quires a transient pulse of fluids from a deep source to activate brittle faulting. The main-
20 shock was preceded by two foreshock swarm-like sequences that may be further evidence
21 for fluid movement in a critically loaded fault network. Contrary to plate boundary events,
22 the M_w 6.5 Botswana earthquake did not require prior localized stress or strain accumula-
23 tion. We propose that the crust in SCR, even long after the last tectonic episode, consti-
24 tutes a reservoir of elastic stress that can be released episodically, for instance as a result
25 of deep fluid migration.

26 While earthquakes primarily occur along plate boundaries, where most of the tec-
 27 tonic strain is released, large events also strike stable continental interiors, although much
 28 less frequently [e.g. *Johnston*, 1989; *Calais et al.*, 2016]. The New Madrid region of the
 29 Central U.S., with four $M > 7$ events between December 1811 and February 1812, is a type
 30 locale for large earthquakes in such settings [e.g. *Nuttli*, 1973; *Johnston*, 1996; *Hough*
 31 *et al.*, 2000], and examples can be found in all continents. South Africa was struck in
 32 1969 by the $M_w 6.3$ Ceres earthquake [*Kruger and Scherbaum*, 2014], and in 1998, the
 33 Tennant Creek sequence of M_s 6.3, 6.4, and 6.7 events shook central Australia [*Bow-*
 34 *man*, 1992]. Careful studies of such rare events are important as the mechanism leading to
 35 stress release on faults in regions of very low tectonic deformation remains poorly under-
 36 stood, leading to large uncertainties in hazard assessment in populated continental interiors
 37 [e.g. *Allman and Smolka*, 2001; *Liu and Stein*, 2016]. We focus on the largest stable conti-
 38 nental interior earthquake since the 1998 Tennant Creek events, a M_w 6.5 normal-faulting
 39 earthquake that ruptured a blind fault in Botswana on April 3rd, 2017, within the Kalahari
 40 cratonic domain, far from any identified active fault (Fig. 1).

41 The $M_w 6.5$ Botswana earthquake occurred close to the junction between the Archean
 42 Kaapval craton and the Paleoproterozoic Mahalapye granite of the Limpopo belt (Fig. 1).
 43 It may have reactivated one of the high angle faults that mark the boundary between these
 44 old and seismically quiet geological units [*Kolawole et al.*, 2017]. Seismic activity in its
 45 epicentral region (-25° to -21° south, 23° to 27° east) is more elevated than typical stable
 46 continental interiors, with 23 earthquakes of magnitude larger than 4 detected since Jan-
 47 uary 1st, 2000. The mainshock was followed by about 30 aftershocks of magnitude greater
 48 than 3, as reported by the International Seismological Center (ISC). Aftershocks appear to
 49 first extend over a large region before focusing closer to the epicenter, though this may be
 50 biased by the location capability of small events at teleseismic distances. One of the ob-
 51 jectives of this study is to expand this aftershock catalog and, more importantly, to search
 52 for potential foreshocks, using for the first time a template matching technique at teleseis-
 53 mic distances from the mainshock.

54 Although southern Africa experiences diffuse, low magnitude seismicity [e.g. *Pastier*
 55 *et al.*, 2017], no active structure has been identified in the epicentral region of the Botswana
 56 earthquake. The nearest active faults are 350 km to the north bounding the isolated Oka-
 57 vango tectonic basin, where a $M 6.7$ earthquake occurred in 1952 [*Modisi et al.*, 2000;
 58 *Reeves*, 1972]. This basin has been interpreted by some as an incipient rift at the western

59 end of a belt of weak seismicity that extends from the Okavango basin through the Kariba
 60 graben to the east and connects to the Rukwa region of the East African Rift [*Scholz*
 61 *et al.*, 1976; *Modisi et al.*, 2000], although that interpretation has recently been challenged
 62 [*Pastier et al.*, 2017]. The 2017 Bostwana earthquake is located well away from these
 63 structures. Its GCMT mechanism and fault plane solutions derived from Differential In-
 64 SAR data show a fault plane striking perpendicular to this possible direction of rift prop-
 65 agation [*Kolawole et al.*, 2017; *Albano et al.*, 2017]. However, these published InSAR-
 66 derived fault models did not explore the whole range of possible fault planes and another
 67 objective of this study is to re-evaluate the source mechanism and depth of this earth-
 68 quake.

69 In the following, we show that the Bostwana earthquake (1) occurred at a depth of
 70 29 km, in the lower crust, on a 73° or a 17°-dipping fault, and (2) was preceded by two
 71 foreshock sequences. We argue that this earthquake sequence was triggered by a local and
 72 transient pulse of elevated pore fluid pressure in a lower crust where viscous deformation
 73 should otherwise prevail.

74 **1 InSAR analysis and Bayesian source parameters estimation**

75 We compute an interferogram from Sentinel-1 acquisitions in interferometric wide-
 76 swath mode on March 30th and April 11th 2017 along ascending orbits (see Supp. Mat.).
 77 We identify surface displacements resulting from this normal faulting event as the oval-
 78 shaped set of fringes located in the epicentral region (Fig. 2). We measure about 4 cm of
 79 coseismic surface displacement in the satellite Line-Of-Sight (LOS). Given the incidence
 80 angle of the Radar signal in the epicentral region and assuming negligible horizontal mo-
 81 tion, this corresponds to about 6 cm of subsidence.

82 We use a Bayesian formulation to invert for the source parameters of the main-
 83 shock. The goal is to find whether it is possible to discriminate between the 2 possible
 84 fault planes provided by the GCMT solution. We select a subset of the interferogram
 85 and downsample the interferometric phase using a curvature-based quadtree algorithm
 86 [Fig 2 and Supp. Mat. Fig. S1; *Simons et al.*, 2002]. Our model set up includes a sin-
 87 gular fault plane with constant slip embedded in an elastic homogeneous medium. We solve
 88 for the fault centroid position (longitude, latitude and depth), its orientation (strike and
 89 dip), and the amount of slip along dip. We consider its size fixed (10 km along dip and

90 30 km along strike, chosen based on orders of magnitude for M_w 6 earthquakes) as these
 91 size parameters trade-off with slip. In addition, we solve for a constant offset to add to the
 92 InSAR data.

93 Following Bayes' theorem, we write the posterior Probability Density Function (PDF)
 94 of the model, $P(\mathbf{m}|\mathbf{d})$, as proportional to the product of the prior PDF, $P(\mathbf{m})$, and the like-
 95 lihood, $P(\mathbf{d}|\mathbf{m})$, such as

$$P(\mathbf{m}|\mathbf{d}) \propto P(\mathbf{m})P(\mathbf{d}|\mathbf{m}), \quad (1)$$

96 where \mathbf{m} is the vector of model parameters and \mathbf{d} the vector of data to invert (i.e.
 97 here, the downsampled surface displacements from InSAR). We use uniform distributions
 98 for the prior PDF, imposing positivity on slip (i.e., the fault has to be a normal fault). We
 99 use a Gaussian formulation for the likelihood, $P(\mathbf{d}|\mathbf{m})$, that writes

$$P(\mathbf{d}|\mathbf{m}) \propto e^{-\frac{1}{2}(\mathbf{Gm}-\mathbf{d})^T \mathbf{C}_d^{-1}(\mathbf{Gm}-\mathbf{d})}, \quad (2)$$

100 where, \mathbf{G} is the matrix of Green's functions relating source parameters to surface
 101 displacements and \mathbf{C}_d is the data covariance matrix. We build the Green's functions using
 102 Okada's formulation of the surface displacements produced by slip on a rectangular dis-
 103 location [Okada, 1985]. We use the covariance function of the interferogram to build the
 104 data covariance matrix, describing the influence of turbulent tropospheric noise [see Supp.
 105 Mat.; Jolivet *et al.*, 2015].

106 In the present case, the posterior PDF must be multimodal as both southwest- and
 107 northeast-dipping fault planes should be able to fit surface displacements. Using a classic
 108 sampling approach, for instance based on the long-used Metropolis algorithm, will un-
 109 likely resolve directly the complete shape of the PDF as the probability for one Markov
 110 chain to jump between isolated, high probability regions of the model space is very low.
 111 This is likely why a previously published Bayesian model does not show multiple modes
 112 for the posterior PDF, hence multiple possible dip angles [Albano *et al.*, 2017]. Even if
 113 this probability is not null and sampling all regions of the model space should theoretic-
 114 ally be possible with a classic Metropolis algorithm [Xu *et al.*, 2015], a prohibitive num-
 115 ber of steps would be required. Furthermore, it would be difficult to assert the respec-

116 tive importance of each mode. We use instead the AITar sampler, specifically designed for
 117 high dimensional problems and complex PDF sampling (see Supp. Mat.).

118 Our posterior PDF shows four family of models, including two equally likely and
 119 two equally less likely that we separate using a K-mean clustering algorithm (Supp. Fig.
 120 S3). The two most likely families of models have an average depth of 29 ± 4 km, an av-
 121 erage magnitude of 6.54 ± 0.05 and their centroid location is consistent with that from
 122 GCMT. Members from these 2 families only differ by their dip angle, one being on av-
 123 erage $17^\circ \pm 4^\circ$ and the other at $73^\circ \pm 4^\circ$, hence the two possible families of strike angle
 124 at 180° from eachother. These values are similar to those of the conjugate planes of the
 125 GCMT solution, with slightly steeper or shallower dip angles for the steep – and a shallow
 126 – angle planes, respectively. The InSAR derived centroid location and magnitude are con-
 127 sistent within uncertainties with those determined by GCMT. We will not further consider
 128 the less likely families as their fault strike and magnitude, centroid location, and depth are
 129 not consistent with the seismologically-derived ones. Finally, our results indicate that it is
 130 not possible to discriminate between a steep and a shallow angle normal faulting event as
 131 both families of models are equiprobable.

132 **2 Aftershocks and foreshocks detection**

133 We then seek to detect aftershocks and possible foreshocks of the Botswana earth-
 134 quake. Since no data from local seismic networks were available at the time of this work,
 135 we apply template matching to continuous signals recorded at teleseismic distances (1200
 136 to 2000 km) to the mainshock from November 2016 to April 2017. This technique has
 137 been used to detect low frequency earthquakes (LFE) within tremor signals [*Shelly et al.*,
 138 2007] or to recover missing events in aftershock [*Lengliné and Marsan, 2009; Peng and*
 139 *Zhao, 2009*] and foreshock sequences [*Bouchon et al., 2011; Kato et al., 2012; Lengliné*
 140 *et al., 2012; Kato and Nakagawa, 2014; Gardonio, 2017*]. It is however more challeng-
 141 ing at teleseismic distances because of the much lower signal-to-noise ratio of the seismic
 142 records compared to near-field observations.

143 We select as templates 18 $M > 3$ aftershocks that occurred in the week following the
 144 main event to compute their coherence with continuous seismic records at five teleseismic
 145 stations (Fig. 1). We obtain a continuous record of the coherence per template and per
 146 day. We define a coherence threshold above which we consider that an event has been de-

147 tected (see Supp. Mat.). Figure 3 shows the cumulative number of events detected at least
 148 at 2 teleseismic stations using coherence thresholds of 0.89, 0.9, and 0.91 after removing
 149 auto-detections, i.e. detections of a template by itself. As expected, the number of detec-
 150 tions increases with decreasing threshold. All events are seismic in origin but some of the
 151 lower-threshold ones are located up to 35 km away from the mainshock epicenter, suggest-
 152 ing a fairly broad seismically active region both before and after the mainshock. We also
 153 observe, for all detection thresholds, an increase in seismicity between December 4th and
 154 30th, 2016 – four months before the main event – while only one M4.1 earthquake was
 155 reported by the ISC within 120 km of the main shock during that same time interval.

156 At the 0.91 coherence threshold, we detect a total of 20 new events (see Supp. Mat.).
 157 We manually checked these detections for each station. This number is expectedly much
 158 smaller than near-field template matching studies [*Kato et al.*, 2012; *Lengliné et al.*, 2012;
 159 *Kato and Nakagawa*, 2014] but nevertheless shows a remarkable temporal distribution,
 160 with two sequences of foreshocks. The first one occurs between 4 and 3 months before
 161 the mainshock, with 9 events detected by templates south-west of the mainshock epicen-
 162 ter (Supp. Mat. Fig. S4). Its is followed by a seismically quiet time interval until early
 163 March. The second foreshock sequence occurs during the 2 weeks that precede the main
 164 event, with 5 events detected by three templates north-west of the mainshock.

165 **3 A precursory geodetic signal?**

166 By reference to other preparatory phases identified before large earthquakes, the
 167 foreshocks detected here may be embedded in a broader aseismic event [*Ruiz et al.*, 2014;
 168 *Bouchon et al.*, 2011]. In order to detect such an event, we processed all available Sentinel-
 169 1 acquisitions between April 2015 and August 2017 (Supp. Mat.). The resulting time
 170 series of relative surface displacements between the epicentral region (< 10 km from
 171 the epicenter) and the far-field (> 60 km from the epicenter) shows no significant signal
 172 within the precursory phase during which small earthquakes are detected (Fig. 3). The
 173 same holds for the full time series (Supp. Fig. S8 to S11). The coseismic signal is well
 174 recovered, with a 2-3 cm offset at the time of the main shock. Averaging over the last 11
 175 acquisitions of the time series suggests that the coseismic offset is followed by up to 1 cm
 176 of post-seismic displacements.

177 **4 Present-day regional strain accumulation?**

178 The location of the Botswana earthquake far from areas of concentrated seismic ac-
 179 tivity, in a region with no morphological evidence of recent tectonic activity, raises the
 180 question of present-day strain accumulation in southern Africa. The low strain rates ex-
 181 pected in such an intraplate setting may be difficult to measure geodetically, especially
 182 since the distribution of GPS stations is sparse and uneven. Nevertheless, it is useful to try
 183 place an upper-bound on regional strain accumulation using the existing permanent GPS
 184 stations. We therefore updated the analysis of data from openly available, continuously-
 185 recording GPS stations in southern Africa to derive a continental-scale velocity field in
 186 order to search for region-wide deformation (Supp. Mat. and Fig. 1).

187 We search for deviations from a purely rigid behavior by estimating a single rigid
 188 rotation for the whole region considered here and examining residual velocities. We find
 189 no spatial pattern in residual velocities with respect to a rigid plate (Fig. 1) with an RMS
 190 misfit of 0.25 mm/yr (maximum residual of 0.95 mm/yr), and a χ^2 of 1.1. The compar-
 191 ison of the distribution of residual velocities, normalized by their uncertainty, with that
 192 of a two-dimensional, unit variance, normal distribution shows that the velocities are well
 193 described by a random process (Fig. 1). Although the uneven geographic distribution of
 194 GPS stations in southern Africa is not optimal for this type of study, our results rule out
 195 the possibility of broad-scale deformation at a level of 0.25 mm/yr, consistent with obser-
 196 vations in several other plate interiors [*Nocquet, 2012; Tregoning et al., 2013; Craig and*
 197 *Calais, 2014*], as well as previous results in the same region [*Hackl et al., 2011; Saria*
 198 *et al., 2014*].

199 **5 What caused the Botswana earthquake?**

200 The 2017, M_w 6.5, Botswana earthquake occurred in an area with no previous evi-
 201 dence of similar magnitude events, low and diffuse background seismicity, and no topo-
 202 graphic features indicative of repeated recent faulting, characteristics that are shared by
 203 most large earthquakes in stable continental regions [*Calais et al., 2016*]. That the earth-
 204 quake focal mechanism shows purely normal faulting is consistent with the occurrence of
 205 other normal faulting earthquakes within stable southern Africa [*Heidbach et al., 2016*]
 206 and with stress models derived from horizontal gradients of gravitational potential energy
 207 [*Coblentz and Sandiford, 1994; Stamps et al., 2014*]. Both indicate an extensional stress

208 state with a subvertical maximum principal compressive stress (σ_1) and a subhorizontal
 209 least principal compressive stress (σ_3).

210 However, a striking feature of the event is its depth, which all authors consistently
 211 find between 25 and 30 km, well into the lower part of a crust that is around 35 km-thick
 212 in the epicentral area [*Nguuri et al.*, 2001; *Tedla et al.*, 2011; *Youssof et al.*, 2013]. The
 213 occurrence of earthquakes in the lower crust is often interpreted as evidence for a mafic
 214 composition [*Shudofsky et al.*, 1987; *Nyblade and Langston*, 1995; *Albaric et al.*, 2008;
 215 *Craig et al.*, 2011]. Seismic data in the Kaapval craton however show a low Poisson ratio
 216 of 0.25 for the whole crust and a 2,860 kg/m³ lowermost crust density, indicative of a fel-
 217 sic composition [*James et al.*, 2003], consistent with the lack of mafic granulite xenoliths
 218 from the lower Kaapvaal crust [*Schmitz and Bowring*, 2003].

219 Given a crustal geotherm derived from local surface heat flow measurements, crustal
 220 yield strength envelopes for the region (Fig. 4a) show that brittle failure should not hap-
 221 pen at such depth, under hydrostatic pore-fluid pressure, as a felsic lower crust flows at
 222 low differential stress. In the absence of a mafic lower crust, (1) the maximum differential
 223 stress that can be maintained at hypocentral depth is about 50-100 MPa and (2) deforma-
 224 tion at such depth is controlled by viscous flow. However, if pore-fluid pressure becomes
 225 sub-lithostatic, brittle failure on a 73°-dip fault is allowed at a differential stress lower than
 226 50 MPa (Fig. 4c). Alternate mechanisms are also possible, such as thermal shear runaway,
 227 rupture of a brittle asperity, or dehydration reactions [e.g. *Green and Houston*, 1995; *Pri-
 228 eto et al.*, 2013]. The former two require significant, on-going, shear motion, which is
 229 unlikely in this stable cratonic environment. The latter implies a phase transition, which
 230 would require a recent rejuvenation of the cratonic crust that is not documented. The sta-
 231 bility of the cratonic crust requires an external forcing to trigger this event.

232 Therefore, a likely explanation for the Botswana earthquake is that it was triggered
 233 by elevated, sub-lithostatic, pore fluid pressure that enabled failure at the low differen-
 234 tial stress that prevails in the viscous lower crust [*Gold and Soter*, 1985]. The observed
 235 foreshock swarm-like sequences may be the signature of the initiation of a pulse of high
 236 pore fluid pressure [*Hainzl and Fischer*, 2002; *Reyners et al.*, 2007; *Balfour et al.*, 2015].
 237 Field observations show numerous evidence of fluid-assisted embrittlement in the vis-
 238 cous regime of deformation [*Handy et al.*, 2007; *Wehrens et al.*, 2016]. Lower-crustal
 239 earthquakes in the northern Alpine foreland [*Deichmann*, 1992] and beneath the Flinders

240 Ranges of South Australia [*Balfour et al.*, 2015] have been interpreted as the result of a
 241 decrease of effective stress on pre-existing faults by fluids at near-lithostatic pore pressure,
 242 allowing a switch from viscous to brittle deformation. In the later case, the authors argued
 243 for a deep fluid source from a remnant hydrated mantle on the basis of elevated $^3\text{He}/^4\text{He}$
 244 ratios in springs, as also observed in Vogtland, Bohemia, and Eger Rift intraplate seismic-
 245 ity areas of Central Europe [*Weise et al.*, 2001; *Bräuer et al.*, 2009]. In the Taupo active
 246 rift (New Zealand), lower-crustal earthquakes in the viscous regime are interpreted as trig-
 247 gered by fluids migrating upward from the hydrated Hikurangi subduction mantle wedge
 248 [*Reyners et al.*, 2007].

249 Southern Africa is a largely cratonic province characterized by widespread kim-
 250 berlite outcrops, which take their source in carbonate-rich matrices and parental magma
 251 [*Kamenetsky et al.*, 2014]. Rapid kimberlite melt ascent through the crust is assumed to
 252 be driven by the exsolution of a H_2O - and CO_2 -rich fluid phases at mantle depths [*Russell*
 253 *et al.*, 2012]. This requires the presence of volatiles in the mantle, which can be hosted
 254 in the lower lithosphere until remobilization under large-scale tensional tectonic stresses
 255 as shown in the Virunga volcanic field of the East African Rift [*Hudgins et al.*, 2015]. In
 256 the Okavango basin, 350 km north of the Botswana earthquake, a thermal anomaly mea-
 257 sured in the absence of surface magmatism and of a thinned or altered lithosphere is in-
 258 terpreted as the signature of fluids advected from a metasomatized lithospheric mantle
 259 [*Leseane et al.*, 2015]. Therefore, several lines of evidence point to the presence of signif-
 260 icant amounts of fluids in the upper mantle underneath southern and eastern Africa. The
 261 upward migration of these deep and buoyant fluids could perhaps explain the locally el-
 262 evated pore-fluid pressure necessary to trigger seismicity in the otherwise ductile lower
 263 crust of the Kaapval craton.

264 **6 Conclusion**

265 The occurrence of the April 3rd, 2017, Botswana earthquake in a felsic lower crust
 266 where viscous deformation should prevail indicates that pore-fluid pressure elevated to
 267 sub-lithostatic played a key role in triggering the rupture. The two swarm-like sequences
 268 of earthquakes that preceded the main Botswana event in December and March 2017 may
 269 be further evidence for fluid movement in a critically loaded fault network, that eventually
 270 led to a large event. Finally, the damage caused by the mainshock potentially led to a de-

crease in pore-fluid pressure locally, turning off the activity of this swarm-like sequence,
hence the detection of a classic Omori decay of aftershock productivity.

The Botswana earthquake therefore did not require localized, present-day, stress or strain accumulation, contrary to plate boundary events resulting from the near-fault accrual of stress imposed by plate and block motions [Kanamori and Brodsky, 2004]. In a pre-stressed crust able to store reversible strain on long timescales [Feldl and Bilham, 2006; Craig *et al.*, 2016] with faults at or close to failure [Townend and Zoback, 2000], short-term fault strength transients, such as those triggered by fluids leaks from the upper mantle, may be all it takes to trigger large events.

Acknowledgments

We thank IRIS for granting access to seismic data (<http://ds.iris.edu/SeismiQuery>). Sentinel 1A and B acquisitions were downloaded through the Plateforme d'Exploitation des Produits Sentinel (PEPS, <https://peps.cnes.fr>) of the Centre National des Études Spatiales (CNES). The seismic catalog was downloaded through the ISC website (<http://www.isc.ac.uk/>). Global Precipitation Measurement data are available for download at <https://pmm.nasa.gov/GPM>. BG received funding from the European Research Council (ERC) under the European Union's Horizon 2020 research and innovation program (REALISM project, grant agreement 681346). RJ received funding from the European Research Council (ERC) under the European Union's Horizon 2020 research and innovation program (Geo-4D project, grant agreement 758210). EC acknowledges support from the Institut Universitaire de France and from the INSU/CNRS Tellus-Rift program. We thank K. Materna and an anonymous reviewer for the time they took at evaluating our work and their constructive comments.

References

- Albano, M., M. Polcari, C. Bignami, M. Moro, M. Saroli, and S. Stramondo (2017), Did anthropogenic activities trigger the 3 april 2017 mw 6.5 botswana earthquake?, *Rem. Sens.*, 9(12), doi:10.3390/rs9101028.
- Albaric, J., J. Déverchère, C. Petit, J. Perrot, and B. Le Gall (2008), Crustal rheology and depth distribution of earthquakes: Insights from the central and southern East African Rift System, *Tecton.*, 468(1-4), 28–41.
- Allman, A., and A. Smolka (2001), Increasing Loss Potential in Earthquake Risk-A Reinsurance Perspective, in *Proceedings of the Workshop: Evaluation of the potential for large*

- 302 *earthquakes in regions of present-day low seismic activity in Europe*, edited by T. Camel-
303 beeck, pp. 1–4.
- 304 Balfour, N. J., P. R. Cummins, S. Pilia, and D. Love (2015), Localization of intraplate de-
305 formation through fluid-assisted faulting in the lower-crust: The Flinders Ranges, South
306 Australia, *Tecton.*, 655(C), 97–106, doi:10.1016/j.tecto.2015.05.014.
- 307 Ballard, S., H. N. Pollack, and N. J. Skinner (1987), Terrestrial heat flow in Botswana and
308 Namibia, *J. Geophys. Res.*, 92(B7), 6291–6300.
- 309 Bouchon, M., H. Karabulut, M. Aktar, S. Ozalaybey, J. Schmittbuhl, and M. Bouin (2011),
310 Extended nucleation of the 1999 Mw 7.6 Izmit earthquake, *Science*, 331, doi:10.1126/
311 science.1197341.
- 312 Bowman, J. R. (1992), The 1988 Tennant Creek, northern territory, earthquakes: A syn-
313 thesis, *Aust. J. Earth Sci.*, 39(5), 651–669.
- 314 Bräuer, K., H. Kämpf, and G. Strauch (2009), Earthquake swarms in non-volcanic re-
315 gions: What fluids have to say, *Geophys. Res. Lett.*, 36(17), 481–5, doi:10.1029/
316 2009GL039615.
- 317 Byerlee, J. (1978), Friction of rocks, *Pure Appl. Geophys.*, 116(4-5), 615–626.
- 318 Calais, E., T. Camelbeek, S. Stein, M. Liu, and T. J. Craig (2016), A new paradigm
319 for large earthquakes in stable continental plate interiors, *Geophys. Res. Lett.*, 43(20),
320 10,621–10,637, doi:10.1002/2016GL070815.
- 321 Coblentz, D. D., and M. Sandiford (1994), Tectonic stresses in the African plate: Con-
322 straints on the ambient lithospheric stress state, *Geology*, 22(9), 831–834.
- 323 Craig, T. J., and E. Calais (2014), Strain accumulation in the New Madrid and Wabash
324 Valley seismic zones from 14 years of continuous gps observation, *J. Geophys. Res.*
325 *Solid Earth*, 119, 9110–9129, doi:10.1002/2014JB011498.
- 326 Craig, T. J., J. A. Jackson, K. Priestley, and D. McKenzie (2011), Earthquake distribution
327 patterns in Africa: their relationship to variations in lithospheric and geological struc-
328 ture, and their rheological implications, *Geophys. J. Int.*, 185(1), 403–434.
- 329 Craig, T. J., E. Calais, L. Fleitout, L. Bollinger, and O. Scotti (2016), Evidence for the re-
330 lease of long-term tectonic strain stored in continental interiors through intraplate earth-
331 quakes, *Geophys. Res. Lett.*, 43, 6826–6836, doi:10.1002/2016GL069359.
- 332 Deichmann, N. (1992), Structural and rheological implications of lower-crustal earthquakes
333 below northern Switzerland, *Phys. Earth Planet. Inter.*, 69, 270–280.

- 334 Ekström, G., M. Nettles, and A. M. Dziewonski (2012), The global CMT project 2004-
 335 2010: Centroid-moment tensors for 13,017 earthquakes, *Phys. Earth Planet. Inter.*, pp.
 336 200–201, doi:10.1016/j.pepi.2012.04.002.
- 337 Farr, T. G., and M. Kobrick (2000), Shuttle radar topography mission produces a wealth of
 338 data, *Eos Trans. AGU*, *81*(48), 583–585.
- 339 Feldl, N., and R. Bilham (2006), Great Himalayan earthquakes and the Tibetan plateau,
 340 *Nature*, *444*(7116), 165–170, doi:10.1038/nature05199.
- 341 Gardonio, B. (2017), Seismic and aseismic slip: the japanese subduction zone, Ph.D. the-
 342 sis, Université Savoie Mont Blanc.
- 343 Gold, T., and S. Soter (1985), Fluid ascent through the solid lithosphere and its relation to
 344 earthquakes, *Pure Appl. Geophys.*, *122*(2-4), 492–530.
- 345 Green, H. W., and H. Houston (1995), The Mechanics of Deep Earthquakes, *Ann. Rev.*
 346 *Earth Planet. Sci.*, *23*(1), 169–213, doi:10.1146/annurev.ea.23.050195.001125.
- 347 Hackl, M., R. Malservisi, U. Hugentobler, and R. Wonnacott (2011), Estimation of ve-
 348 locity uncertainties from GPS time series: Examples from the analysis of the South
 349 African TrigNet network, *J. Geophys. Res.*, *116*(B11), B11,404–12.
- 350 Hainzl, S., and T. Fischer (2002), Indications for a successively triggered rupture growth
 351 underlying the 2000 earthquake swarm in Vogtland/NW Bohemia, *J. Geophys. Res. Solid*
 352 *Earth*, *107*(B12), ESE 5–1–ESE 5–9.
- 353 Handy, M., G. Hirth, and R. Burgmann (2007), Continental fault structure and rheology
 354 from the frictional-to-viscous transition downward, In: *Handy, M.R., Hirth, G., Hovius,*
 355 *N. (Eds.), Tectonic Faults: Agents of Change on a Dynamic Earth. MIT, Cambridge, MA,*
 356 pp. 139–181.
- 357 Heidbach, O., M. Rajabi, K. Reiter, M. Ziegler, and W. Team (2016), World stress map
 358 database release 2016, *GFZ Data Services*, doi:http://doi.org/10.5880/WSM.2016.001.
- 359 Hirth, G., C. Teyssier, and J. W. Dunlap (2001), An evaluation of quartzite flow laws
 360 based on comparisons between experimentally and naturally deformed rocks, *Internation-*
 361 *ational Journal of Earth Sciences*, *90*(1), 77–87.
- 362 Hough, S. E., J. G. Armbruster, L. Seeber, and J. F. Hough (2000), On the Modified Mer-
 363 calli intensities and magnitudes of the 1811–1812 New Madrid earthquakes, *J. Geophys.*
 364 *Res Solid Earth*, *105*(B10), 23,839–23,864.
- 365 Hudgins, T. R., S. B. Mukasa, A. C. Simon, G. Moore, and E. Barifaijo (2015), Melt in-
 366 clusion evidence for CO₂-rich melts beneath the western branch of the East African

- 367 Rift: implications for long-term storage of volatiles in the deep lithospheric mantle,
368 *Contributions to Mineralogy and Petrology*, 169, 1–18.
- 369 James, D. E., F. Niu, and J. R. Lithos (2003), Crustal structure of the Kaapvaal craton and
370 its significance for early crustal evolution, *Lithos*, 71, 413–429.
- 371 Johnston, A. C. (1989), The Seismicity of ‘Stable Continental Interiors’, in *Earthquakes*
372 *at North-Atlantic Passive Margins: Neotectonics and Postglacial Rebound*, pp. 299–327,
373 Springer Netherlands, Dordrecht.
- 374 Johnston, A. C. (1996), Seismic moment assessment of earthquakes in stable continental
375 regions—II. Historical seismicity, *Geophys. J. Int.*, 125, 639–678.
- 376 Jolivet, R., M. Simons, P. S. Agram, Z. Duputel, and Z.-K. Shen (2015), Aseismic slip
377 and seismogenic coupling along the central San Andreas Fault, *Geophys. Res. Lett.*,
378 42(2), 297–306, doi:10.1002/2014GL062222.
- 379 Kamenetsky, V. S., A. V. Golovin, R. Maas, A. Giuliani, M. B. Kamenetsky, and Y. Weiss
380 (2014), Towards a new model for kimberlite petrogenesis: Evidence from unaltered
381 kimberlites and mantle minerals, *Earth Science Reviews*, 139(C), 145–167.
- 382 Kanamori, H., and E. E. Brodsky (2004), The physics of earthquakes, *Rep. Prog. Phys.*,
383 67(8), 1429–1496, doi:10.1088/0034-4885/67/8/R03.
- 384 Kato, A., and S. Nakagawa (2014), Multiple slow-slip events during a foreshock sequence
385 of the 2014 Iquique, Chile Mw 8.1 earthquake, *Geophys. Res. Lett.*, 41(15), 5420–5427,
386 doi:10.1002/2014GL061138.
- 387 Kato, A., K. Obara, T. Igarashi, H. Tsuruoka, S. Nakagawa, and N. Hirata (2012), Prop-
388 agation of slow slip leading up to the 2011 Mw 9.0 Tohoku-Oki earthquake, *Science*,
389 335, 705–708, doi:10.1126/science.1215141.
- 390 Kolawole, F., E. A. Atekwana, S. Malloy, D. S. Stamps, R. Grandin, M. G. Abdelsalam,
391 K. Leseane, and E. M. Shemang (2017), Aeromagnetic, gravity, and Differential Inter-
392 ferometric Synthetic Aperture Radar analyses reveal the causative fault of the 3 april
393 2017 Mw6.5 Moiyabana, Botswana, earthquake, *Geophys. Res. Lett.*, 44(17), 8837–8846,
394 doi:10.1002/2017GL074620.
- 395 Kruger, F., and F. Scherbaum (2014), The 29 September 1969, Ceres, South Africa, Earth-
396 quake: Full Waveform Moment Tensor Inversion for Point Source and Kinematic Source
397 Parameters, *Bull. Seis. Soc. Am.*, 104(1), 576–581.
- 398 Lengliné, O., and D. Marsan (2009), Inferring the coseismic and postseismic stress
399 changes caused by the 2004 mw=6 parkfield earthquake from variations of recur-

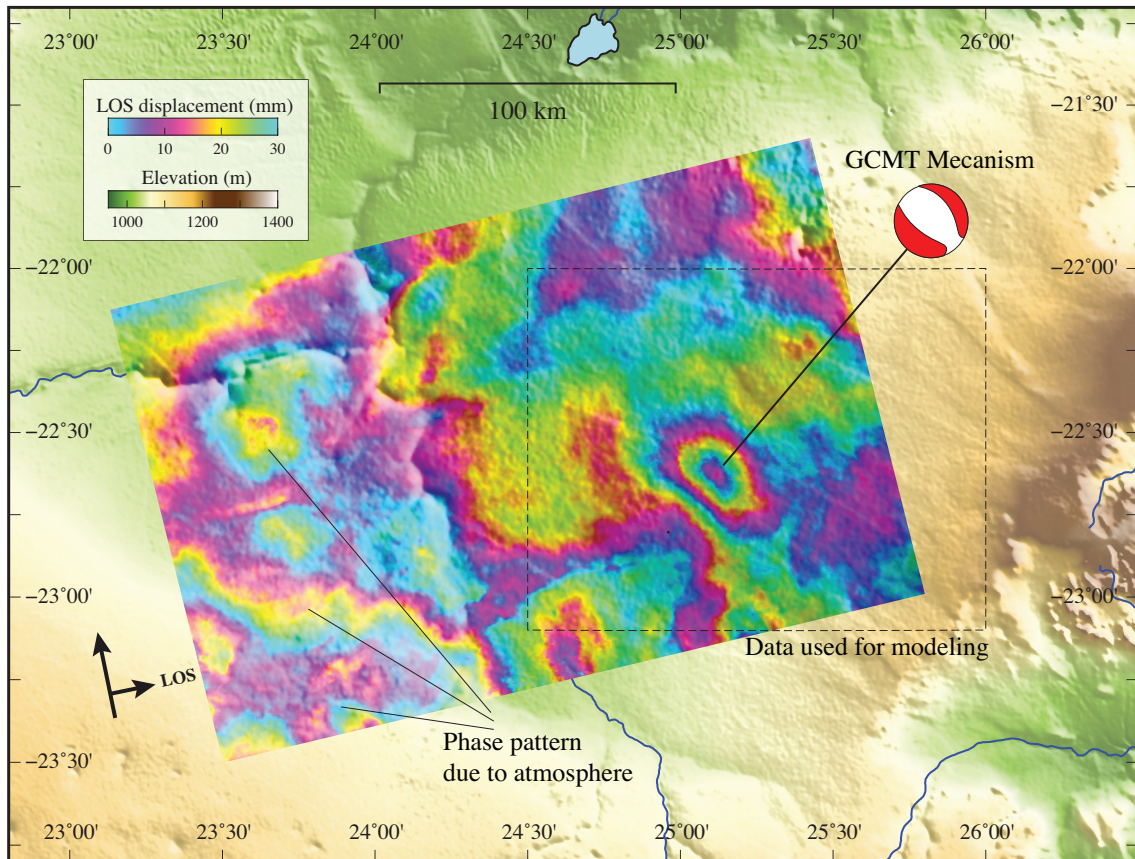
- 400 rence times of microearthquakes, *J. Geophys. Res.*, *114*(B10), 2156–2202, doi:10.1029/
401 2008JB006118.
- 402 Lengliné, O., B. Enescu, Z. Peng, and K. Shiomi (2012), Decay and expansion of the
403 early aftershock activity following the 2011, Mw9.0 Tohoku earthquake, *Geophys. Res.*
404 *Lett.*, *39*(18), 877–6, doi:10.1029/2012GL052797.
- 405 Leseane, K., E. A. Atekwana, K. L. Mickus, M. G. Abdelsalam, E. M. Shemang, and
406 E. A. Atekwana (2015), Thermal perturbations beneath the incipient Okavango Rift
407 Zone, northwest Botswana, *J. Geophys. Res. Solid Earth*, *120*, 1–19.
- 408 Liu, M., and S. Stein (2016), Mid-continental earthquakes: Spatiotemporal occurrences,
409 causes, and hazards, *Earth Science Reviews*, *162*, 364–386.
- 410 Modisi, M. P., E. A. Atekwana, A. B. Kampunzu, and T. H. Ngwisanyi (2000), Rift kine-
411 matics during the incipient stages of continental extension: Evidence from the nascent
412 Okavango rift basin, northwest Botswana, *Geology*, *28*(10), 939–942.
- 413 Nguuri, T. K., J. Gore, D. E. James, S. J. Webb, C. Wright, T. G. Zengeni, O. Gwavava,
414 and J. A. Snoke (2001), Crustal structure beneath southern Africa and its implications
415 for the formation and evolution of the Kaapvaal and Zimbabwe cratons, *Geophys. Res.*
416 *Lett.*, *28*(13), 2501–2504, doi:10.1029/2000GL012587.
- 417 Nocquet, J. M. (2012), Present-day kinematics of the Mediterranean: A comprehensive
418 overview of GPS results, *Tecton.*, *578*, 220–242.
- 419 Nuttli, O. W. (1973), The Mississippi Valley earthquakes of 1811 and 1812: Intensities,
420 ground motion and magnitudes, *Bull. Seis. Soc. Am.*, *63*(1), 227–248.
- 421 Nyblade, A. A., and C. A. Langston (1995), East African earthquakes below 20 km depth
422 and their implications for crustal structure, *Geophys. J. Int.*, *121*, 49–62.
- 423 Okada, Y. (1985), Surface deformation due to shear and tensile faults in a half-space, *Bull.*
424 *Seismol. Soc. Am.*, *75*(4), 1135–1154.
- 425 Pastier, A.-M., O. Dauteuil, M. Murray-Hudson, F. Moreau, A. Walpersdorf, and
426 K. Makati (2017), Is the Okavango Delta the terminus of the East African Rift System?
427 Towards a new geodynamic model: Geodetic study and geophysical review, *Tecton.*,
428 *712-713*(C), 469–481.
- 429 Peng, Z., and P. Zhao (2009), Migration of early aftershocks following the 2004 parkfield
430 earthquake, *Nat. Geosci.*, *2*, 877–881, doi:10.1038/ngeo697.
- 431 Prieto, G. A., M. Florez, S. A. Barrett, G. C. Beroza, P. Pedraza, J. F. Blanco, and
432 E. Poveda (2013), Seismic evidence for thermal runaway during intermediate-depth

- 433 earthquake rupture, *Geophysical Research Letters*, 40(23), 6064–6068, doi:10.1002/
434 2013GL058109.
- 435 Reeves, C. V. (1972), Rifting in the Kalahari?, *Nature*, 237(5350), 95–96.
- 436 Reyners, M., D. Eberhart-Phillips, and G. Stuart (2007), The role of fluids in lower-crustal
437 earthquakes near continental rifts, *Nature*, 446(7139), 1075–1078.
- 438 Ruiz, S., M. Metois, A. Fuenzalida, J. Ruiz, F. Leyton, R. Grandin, C. Vigny,
439 R. Madariaga, and J. Campos (2014), Intense foreshocks and a slow slip event pre-
440 ceded the 2014 Iquique Mw 8.1 earthquake, *Science*, 345(6201), 1165–1169, doi:
441 10.1126/science.1256074.
- 442 Russel, J. K., and M. G. Kopylova (1999), A steady state conductive geotherm for the
443 north central Slave, Canada: Inversion of petrological data from the Jericho Kimberlite
444 pipe, *J. Geophys. Res.*, 104(B4), 7089–7101.
- 445 Russell, J. K., L. A. Porritt, Y. Lavallée, and D. B. Dingwell (2012), Kimberlite ascent by
446 assimilation-fuelled buoyancy, *Nature*, 481(7381), 352–356.
- 447 Rutter, E. H., and K. H. Brodie (2004), Experimental intracrystalline plastic flow in hot-
448 pressed synthetic quartzite prepared from Brazilian quartz crystals, *J. Struct. Geol.*,
449 26(2), 259–270.
- 450 Saria, E., E. Calais, D. S. Stamps, D. Delvaux, and C. Hartnady (2014), Present-day kine-
451 matics of the East African Rift, *J. Geophys. Res. Solid Earth*, 119(4), 3584–3600.
- 452 Schmitz, M. D., and S. A. Bowring (2003), Ultrahigh-temperature metamorphism in the
453 lower crust during Neoproterozoic Ventersdorp rifting and magmatism, Kaapvaal Craton,
454 southern Africa, *GSA Bull.*, 115(5), 533–548.
- 455 Scholz, C. H., T. A. Koczyński, and D. G. Hutchins (1976), Evidence for incipient rifting
456 in southern Africa, *Geophysical Journal of the Royal Astronomical Society*, 44(1), 135–
457 144, doi:10.1111/j.1365-246X.1976.tb00278.x.
- 458 Shelly, D., G. Beroza, and S. Ide (2007), Non-volcanic tremor and low-frequency earth-
459 quake swarms, *Nature*, 446, 305–307, doi:10.1038/nature05666.
- 460 Shudofsky, G. N., S. Cloetingh, S. Stein, and R. Wortel (1987), Unusually deep earth-
461 quakes in East Africa: Constraints on the thermo-mechanical structure of a continental
462 rift system, *Geophys. Res. Lett.*, 14(7), 741–744.
- 463 Sibson, R. H. (1989), High-angle reverse faulting in northern New Brunswick, Canada,
464 and its implications for fluid pressure levels, *J. Struct. Geol.*, 11(7), 873–877.

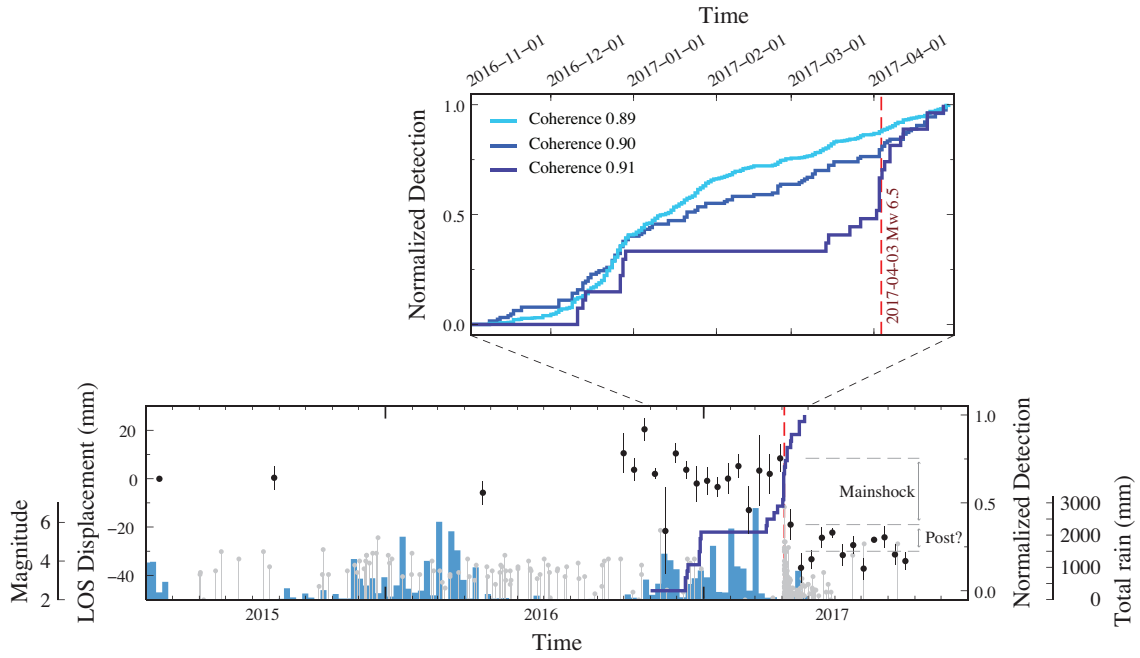
- 465 Simons, M., Y. Fialko, and L. Rivera (2002), Coseismic deformation from the 1999 mw
466 7.1 hector mine, california, earthquake as inferred from insar and gps observations,
467 *Bull. Seis. Soc. Am.*, 92(4), 1390–1402, doi:10.1785/0120000933.
- 468 Stamps, D. S., L. M. Flesch, and E. Calais (2014), Current kinematics and dynamics of
469 Africa and the East African Rift System, *J. Geophys. Res.*, 119(6), 5161–5186, doi:10.
470 1002/2013JB010717.
- 471 Tedla, G. E., M. v. d. Meijde, A. A. Nyblade, and F. D. v. d. Meer (2011), A crustal thick-
472 ness map of Africa derived from a global gravity field model using Euler deconvolu-
473 tion, *Geophys. J. Int.*, 187(1), 1–9, doi:10.1111/j.1365-246X.2011.05140.x.
- 474 Townend, J., and M. D. Zoback (2000), How faulting keeps the crust strong, *Geology*,
475 28(5), 399–402.
- 476 Tregoning, P., R. Burgette, S. C. McClusky, S. Lejeune, C. S. Watson, and H. McQueen
477 (2013), A decade of horizontal deformation from great earthquakes, *J. Geophys. Res*
478 *Solid Earth*, 118(5), 2371–2381.
- 479 Wehrens, P., A. Berger, M. Peters, T. Spillmann, and M. Herwegh (2016), Deformation at
480 the frictional-viscous transition: Evidence for cycles of fluid-assisted embrittlement and
481 ductile deformation in the granitoid crust, *Tecton.*, 693(Part A), 66–84.
- 482 Weise, S. M., K. Bräuer, H. Kämpf, G. Strauch, and U. Koch (2001), Transport of mantle
483 volatiles through the crust traced by seismically released fluids: a natural experiment in
484 the earthquake swarm area Vogtland/NW Bohemia, Central Europe, *Tecton.*, 336(1-4),
485 137–150, doi:10.1016/S0040-1951(01)00098-1.
- 486 Xu, W., R. Dutta, and S. Jónsson (2015), Identifying active faults by improving earthquake
487 locations with insar data and bayesian estimation: The 2004 Tabuk (Saudi Arabia)
488 earthquake sequence, *Bull. Seis. Soc. Am.*, 105(2A), 765–775, doi:10.1785/0120140289.
- 489 Youssof, M., H. Thybo, I. M. Artemieva, and A. Levander (2013), Moho depth and crustal
490 composition in Southern Africa, *Tecton.*, 609(C), 267–287.

491 **Table 1.** Catalog of the newly detected events. The time of occurrence corresponds to the time at which
 492 coherency between the template and the continuous signal is the highest. The locations of the detected events
 493 are the same as the location of the template they matched, as indicated in the ISC catalog. Magnitudes are
 494 estimated by calculating the amplitude ratio (see Supp. Mat.).

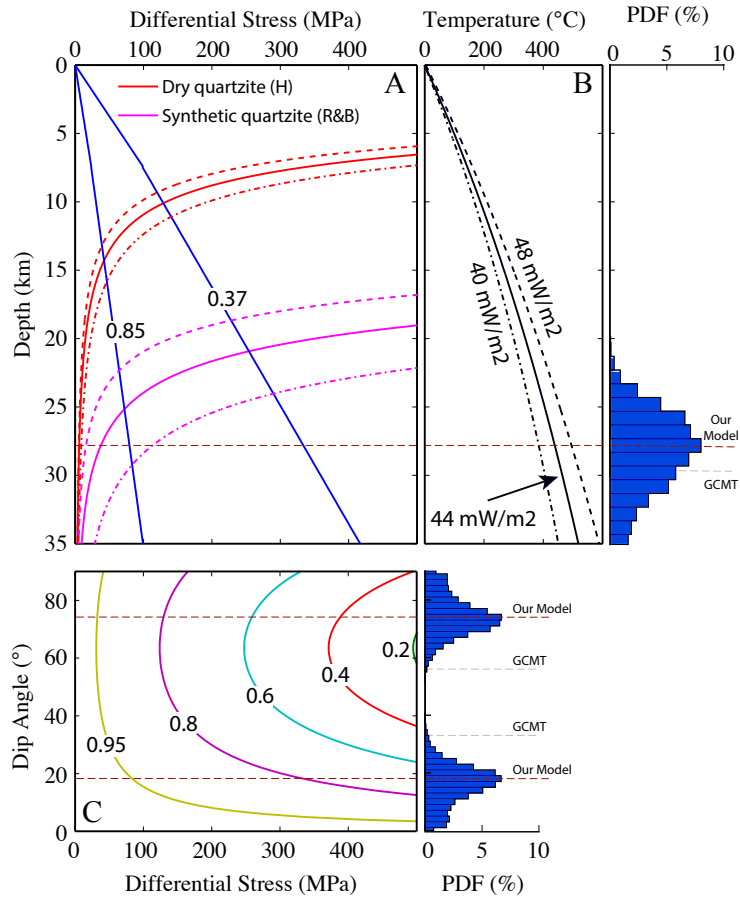
Year	Month	Day	Hour	Minute	Second	Latitude	Longitude	Magnitude
2016	12	11	17	9	32.05	-22.5367	24.9746	3.3
2016	12	11	19	28	14.05	-22.6610	25.0010	3.5
2016	12	13	21	46	46.05	-22.5367	24.9746	3.3
2016	12	14	17	22	52.05	-22.6610	25.0010	3.6
2016	12	27	12	1	44.05	-22.6913	25.1021	3.6
2016	12	27	16	16	18.05	-22.6610	25.0010	3.8
2016	12	28	10	56	54.05	-22.9860	25.1260	3.7
2016	12	28	15	12	22.05	-22.6610	25.0010	3.4
2016	12	29	7	39	24.05	-22.9870	24.9980	3.7
2017	03	14	18	38	20.05	-22.5646	25.0868	3.1
2017	03	15	15	12	2.050	-22.6610	25.0010	3.9
2017	03	23	17	43	12.05	-22.5367	24.9746	3.5
2017	03	27	10	18	4.050	-22.6610	25.0010	3.9
2017	04	02	8	30	40.05	-22.5367	24.9746	3.5
2017	04	05	12	29	10.05	-22.3206	25.4211	3.4
2017	04	11	11	57	32.05	-22.5367	24.9746	3.5
2017	04	12	19	3	28.05	-22.8180	24.9340	3.8
2017	04	21	11	52	4.050	-22.5367	24.9746	3.5
2017	04	21	21	36	48.05	-22.6610	25.0010	3.6
2017	04	27	5	36	56.05	-22.6784	25.1558	3.3



505 **Figure 2. InSAR data** - Interferogram derived from Sentinel 1 acquisitions on March 30th and April
 506 11th, 2017. One color fringe indicates 3 cm of displacement in the satellite Line-Of-Sight (thick black ar-
 507 row). Dotted line rectangle indicates the subset of data used for the Bayesian modeling. Focal mechanism is
 508 from GCMT [Ekström *et al.*, 2012]. Background color is the digital elevation model from SRTM [Farr and
 509 Kobrick, 2000]. Blue lines indicate major rivers.



510 **Figure 3. Template matching detection and InSAR time series - Top** Normalized number of template
 511 detections as a function of time from November 2016 to late April 2017 for three coherence thresholds. The
 512 red dotted line indicates the time of the Botswana M_w 6.5 earthquake. **Bottom** Black dots are the differential
 513 displacement at the time of Sentinel 1 acquisitions between the epicentral region (average of pixels located
 514 less than 10 km away from the maximum displacement) and a stable region (average of pixels located between
 515 50 and 100 km away from the maximum displacement). Blue line is the normalized number of template de-
 516 tections for a coherence threshold of 0.91. Light blue bars are the cumulative rain fall summed over weekly
 517 periods. No obvious relationship can be found between hydrological loads besides the fact that the earthquake
 518 occurred at the end of the rainfall period. Gray lines and dots are earthquake occurrences and their magnitude
 519 from the ISC catalog. Rainfall and earthquakes are considered between 19° and 30° of longitude and 27° and
 520 17° of latitude south.



521 **Figure 4. Mechanical behavior of rocks and earthquake source parameters - A** Red and magenta lines
 522 show dislocation creep flow laws using dry and synthetic quartzite rheologies for three geotherms shown on
 523 panel B. Flow law parameters for wet quartzite are from *Rutter and Brodie* [2004] and for dry quartzite from
 524 [*Hirth et al.*, 2001]. Strain rate is $10 \times 10^{-18} \text{ s}^{-1}$. We use a surface heat flow of 44 mW/m^2 , the average of
 525 four close-by measurements [*Ballard et al.*, 1987], and computed the corresponding crustal geotherm [*Russel*
 526 *and Kopylova*, 1999]. Blue lines show friction law for hydrostatic ($\lambda_V = 0.37$) and sub-lithostatic ($\lambda_V = 0.85$)
 527 pore fluid pressure [*Byerlee*, 1978]. **B** Geotherms derived from a surface heat flow of $44 \pm 10\% \text{ mW/m}^2$
 528 calculated following [*Russel and Kopylova*, 1999]. **C** Differential stress ($\sigma_1 - \sigma_3$) required for frictional reac-
 529 tivation of cohesionless normal faults at 30 km depth as a function of their dip angle for different values of the
 530 pore fluid factor λ_V , following [*Sibson*, 1989]. Lithostatic conditions correspond to $\lambda_V = 1$. Histograms are
 531 the probability density functions of the earthquake source parameters estimated from InSAR data, including
 532 centroid depth and dip angle.

Figure 1.

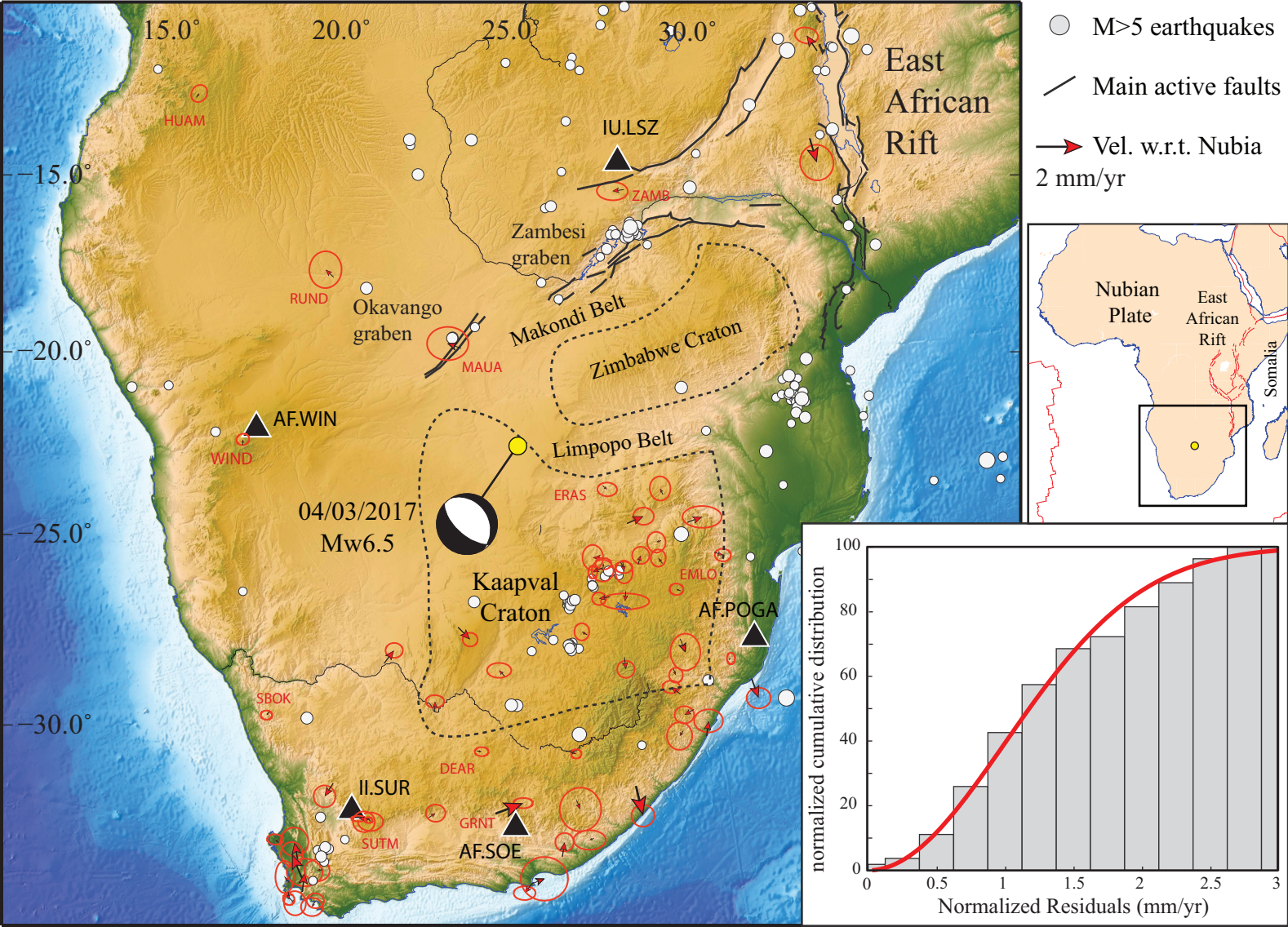


Figure 2.

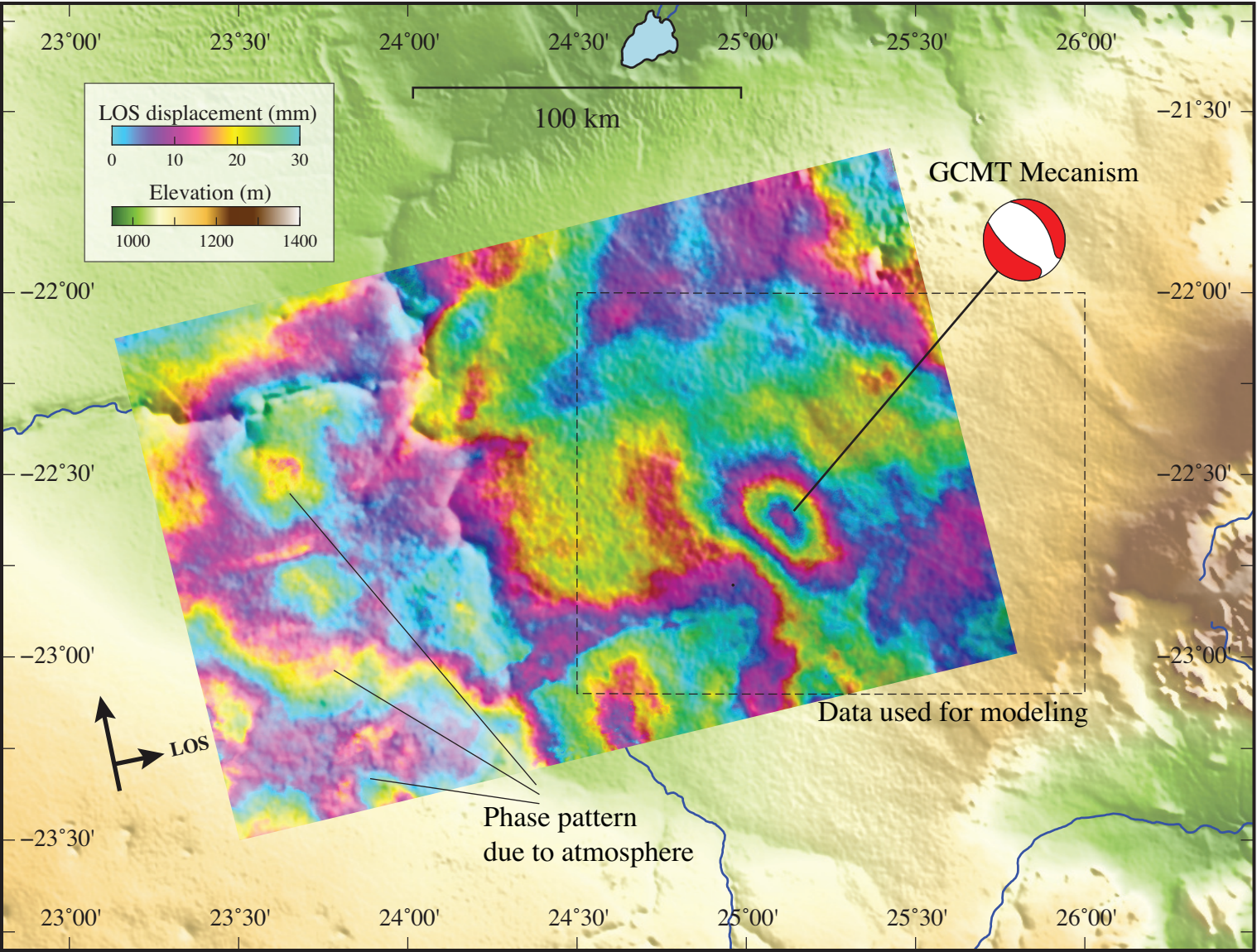


Figure 3.

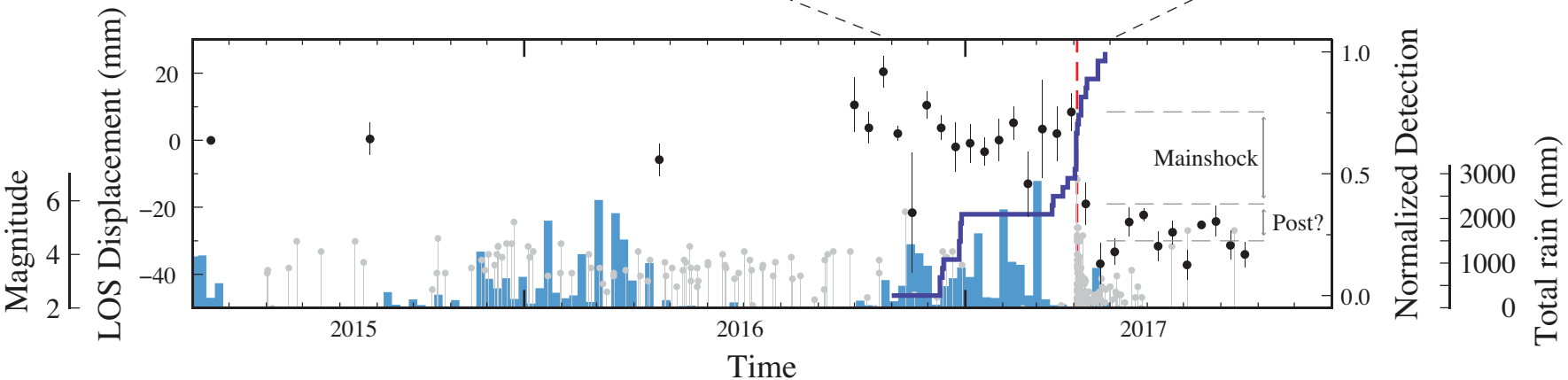
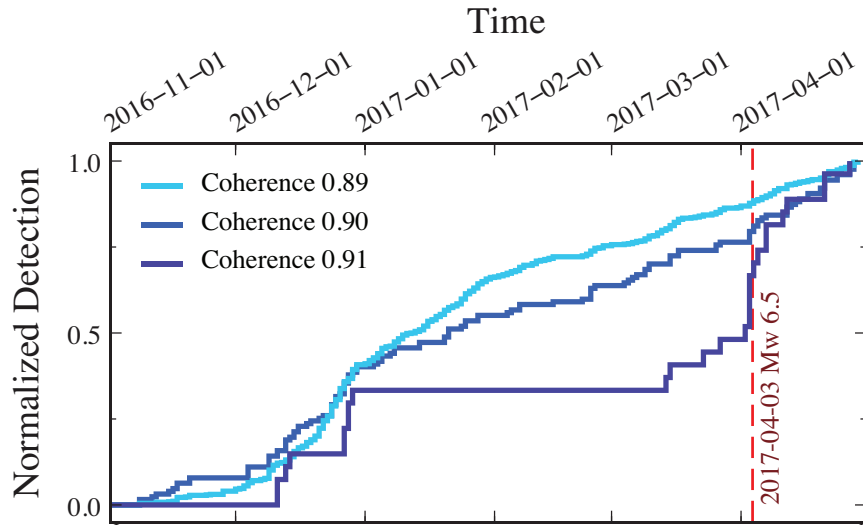


Figure 4.

